THE EFFECT OF REAL-AIR PROPERTIES UPON AERODYNAMIC FORCES, MOMENTS, AND HEAT-TRANSFER RATES FOR REENTRY VEHICLES

By Nathaniel B. Cohen, Ivan E. Beckwith, and Robert L. Trimpi
Langley Research Center

SUMMARY

The effects of the dependence of inviscid flow forces and moments and of aerodynamic heat-transfer rates upon the properties of real air in chemical equilibrium are investigated. It is concluded that equilibrium real-gas effects in general are small except for inviscid forces and moments on some unswept two-dimensional shapes having discontinuities in surface slope and at small angles of attack, and for swept flat plates near the shock detachment angle. Thus, for highly swept configurations at relatively high angles of attack, perfect-gas tests used in conjunction with those analytic studies which are possible should provide useful design data for flight conditions where equilibrium real-gas behavior is expected.

INTRODUCTION

When flight velocities of aircraft and missiles remained below about 3,000 to 4,000 ft/sec in the atmosphere it was permissible to determine aerodynamic and thermodynamic performance by assuming that the air was a perfect gas with constant specific heats. The attainment of considerably higher velocities in the last decade requires the more correct treatment of air as a real gas. The complex chemistry involved in the dissociation and recombination reactions makes simulation of the hypersonic environment more difficult than the low-speed environment, and though shock tubes, shock tunnels, and ballistic ranges have provided much useful data, analytic studies and flight tests must be relied upon to provide much of the necessary information for the determination of real-gas effects at this time. The purpose of the present report is to examine and illustrate the real-gas effects on the inviscid flow forces and moments and upon the aerodynamic heat-transfer rates for some simple shapes in a continuum flow of air in chemical equilibrium. Some comments regarding nonequilibrium flows are included.

The large body of experimental data on the Mark II and III nose cones and the numerical solutions of Gravalos were made available through the

courtesy of the General Electric Missile and Space Vehicle Department.

SYMBOLS

A	constant
C_D	drag coefficient
C_L	lift coefficient
C_m	pitching-moment coefficient
C_p	pressure coefficient
D	drag
H	total enthalpy
h	static enthalpy
h_D	enthalpy in dissociation
L	lift
M	Mach number
m	constant
N_{Le}	Lewis number
N_{Nu}	Nusselt number
N_{Pr}	Prandtl number
N_{Re}	Reynolds number
N_{St}	Stanton number
p	pressure
q	heat-transfer rate

L
1
0
5
0

R	nose radius
R_b	base radius
r	enthalpy recovery factor
T	temperature
t	thickness
u	velocity in x-direction
v	velocity in y-direction
x	surface coordinate in direction of inviscid flow (chordwise coordinate for yawed infinite cylinder)
y	spanwise surface coordinate for yawed infinite cylinder
α	angle of attack
γ	ratio of specific heats or polytropic exponent
γ_e	effective specific-heat ratio
Λ	sweep or yaw angle
μ	viscosity
ξ	axial length
ρ	density
σ	hemisphere angular coordinate, x/R

Subscripts:

aw	adiabatic wall
e	local external to boundary layer
MAX	maximum value
s	stagnation point or line

w   local wall

∞   free stream

INVISCID FLOW OF EQUILIBRIUM AIR

Inviscid flow will be discussed first. Equilibrium thermodynamic properties of air have been extensively and accurately calculated to temperatures of about $15,000^\circ$ K. (See refs. 1 to 5.) With the aid of these results, the inviscid flow forces and moments for a body in an equilibrium real-air flow can be predicted with considerable confidence if the corresponding perfect-gas case is amenable to calculation. However, even the perfect-gas theoretical calculations are limited to comparatively simple shapes at present. Typical of these shapes is the blunt body of revolution, investigated thoroughly in connection with the development of heat-sink types of ballistic missiles.

Blunt-Body Pressure Distributions

As yet, no analytic solutions of the subsonic flow field between the body and the shock have been achieved, but a number of numerical procedures for computing the subsonic and transonic portions of this flow have been derived. These fall into two categories; namely, direct, in which the body shape is given and the shock shape and flow are computed (e.g., refs. 6 and 7), and inverse, in which the shock shape is assumed, and the flow field and body shape are computed (e.g., refs. 8 and 9). Any downstream supersonic flow is computed by the method of characteristics.

The simplest blunt shape, one extensively tested, is the hemisphere. A comparison of experimental pressure-distribution data with predicted distributions is shown for the perfect-gas case in figure 1(a) at Mach numbers near 5. The data were obtained from references 10 to 14, at Mach numbers of 4.15 to 6.80. Predictions shown are the modified Newtonian-Prandtl-Meyer distribution and three of the numerical procedures; namely, those of Gravalos, Edelfelt, and Emmons, $M_\infty = 5.0$ (ref. 6), Belotserkovskii, $M_\infty = 5.8$ (ref. 7) and Van Dyke, $M_\infty = 5.8$ (ref. 8). The three numerical solutions are indistinguishable from one another on this figure and fall slightly lower than the Newtonian-Prandtl-Meyer approximation. Agreement between theory and data is very good, and the modified Newtonian-Prandtl-Meyer distribution appears to be a useful, relatively simple approximation for this shape.

To investigate some of the real-gas effects, the predicted distribution of pressure coefficient over a hemisphere for atmospheric flight at a Mach number of 15 is shown in figure 1(b). The perfect-gas numerical solution up to $x/R \approx 1$ was obtained from the distribution on the blunt portion of a spherically blunted $30°$ half-angle cone given in reference 6. The remainder of the curve, to $\frac{x}{R} = \frac{\pi}{2}$, was estimated on the basis of other high Mach number perfect-gas solutions. The real-gas curve for $M_\infty = 15$ at an altitude of 100,000 feet was computed by the Gravalos method. At this Mach number the predicted real- and perfect-air pressure-coefficient distributions are only slightly different. However, the normalizing real- and perfect-air values of $C_{p,MAX}$, tabulated in the figure, differ by about 3 percent, and this difference is felt in the drag coefficients, which differ by about 2 percent.

Shown also in figure 1(b) are data at $M_\infty = 12$ from X-17 flights R-22 and R-26 (refs. 15 and 16, respectively). These data are compared with the modified Newtonian-Prandtl-Meyer prediction with $M_\infty = 12$ and $\gamma = 1.195$, approximating a real-air distribution (this value of γ is the stagnation-point polytropic exponent for this flight condition). The limited amount of data and this prediction are in good agreement.

The G. E. Mark II nose cone represents another blunt shape on which extensive flight tests have been carried out. This shape has a nearly spherical nose with a conical skirt of $51\frac{1}{2}°$ half-angle. Shown in figure 2 are experimental data for Mach numbers from 11.1 to 16.7 at altitudes of from 74,000 to 102,000 feet, plotted as $C_p/C_{p,MAX}$ against x/R_b. Real-air predictions by Gravalos' method at $M_\infty = 14.6$ and 270,000 feet and at $M_\infty = 10.5$ and about 90,000 feet are shown along with the perfect-gas prediction for $M_\infty = 15$. The experimental data tend to follow the trend of the theoretical predictions but are somewhat lower. The perfect- and real-air predictions at comparable Mach numbers (15 and 14.6, respectively) indicate a significant real-gas effect on the skirt. Elsewhere, predicted real-gas effects on the pressure-coefficient distribution are small.

Downstream Pressures on Blunt Bodies

The requirement for vehicles with better performance than that given by the blunt heat sink led to the second-generation ICBM's, which are relatively slender blunted bodies. To illustrate the real-gas effects upon pressure distribution downstream of the nose regions, figure 3 shows the distribution of $C_p/C_{p,MAX}$ plotted against axial length

for the G. E. Mark III at a Mach number of 20. This missile consists of a spherically blunted 24° half-angle cone followed by an almost cylindrical section (1° converging cone) and a biconic flare. Shown are real-air predictions of Gravalos at 200,000 and 60,430 feet of altitude, the perfect-gas distribution (computed only through the first flare shock), and experimental data at $M_{\infty} = 20$ and an altitude of 62,000 feet. The data, obtained during violent pitching oscillations, generally bracket the prediction.

On the spherical nose the real-gas effects are small, just as on the hemisphere shown earlier, but less noticeable because the abscissa is now axial length rather than surface distance. Downstream, there are more pronounced differences between the distributions, of the order of 20 percent on the main body and 40 percent on the flare. The main difference in pressures, between the real air at 200,000 feet and the real air at 60,000 feet as well as between the real air and perfect air, appears to occur after abrupt body-surface deflections, which on the three-dimensional body surface are still locally two-dimensional Prandtl-Meyer or oblique shock flows. Reflection of waves back onto the body causes a significant part of the pressure differences to disappear.

L
1
0
5
0

Inviscid Forces and Moments on Reentry Vehicles

Lifting reentry vehicles fall generally into two categories, winged vehicles and lifting bodies. Because the inviscid flow fields about these configurations at angles of attack are difficult to compute accurately, simple flows will again be used for illustrative purposes.

The forces and moments on a winged vehicle at positive angles of attack arise mainly from the pressure field on the lower surface. Shown in figure 4 is the ratio of perfect-air to real-air pressure on a swept flat plate plotted against angle of attack up to the perfect-air detachment angle and simulating part of a swept wing at $M_{\infty} = 20$ and an altitude of 200,000 feet. It is evident that real-gas effects are small at small angles of attack, increasing to the order of 20 percent near the perfect-air detachment angles for each sweep. Beyond the detachment angles the pressures cannot be accurately calculated, but measurements indicate that beyond the detachment angles the surface pressures monotonically approach the modified Newtonian predictions. Thus, the ratio $p_{PERFECT}/p_{REAL}$ would be expected to decrease beyond detachment for each value of sweep, reaching the perfect- to real-air stagnation-pressure ratio at an angle of attack of 90° for all sweeps. For the flight conditions of figure 4, this value is 0.95 (shown at the right margin).

The aerodynamic characteristics of a blunted half-cone typify those of a lifting-body configuration. Shown in figure 5 are the characteristics of a spherically blunted 30° half-cone with a bluntness ratio

R/R_b of 0.3 at M_∞ = 15 and an altitude of 85,000 feet. The pressure distributions, shown plotted as p/p_s against dimensionless axial length, were obtained for the complete cone at zero angle of attack by Gravalos (ref. 6), and were assumed to apply to the lower half of this half-cone. The real- and perfect-air curves at a Mach number of 15 may be seen to be little different. With free-stream pressure assumed to be acting on the top surface and with zero base pressure, the aerodynamic characteristics were computed from the pressure distributions with the top surface alined with the stream (α = 0). The results are tabulated in figure 5, from which it is seen that the real-gas effects are generally about 1 percent. Shown also are nose (modified Newtonian-Prandtl-Meyer) and sharp-cone pressures for the same configuration at M_∞ = 20 and 200,000 feet of altitude. Though the performance coefficients were not computed because the pressure distribution is incomplete, the pressures shown indicate real-gas effects of the same order as those shown at M_∞ = 15.

The real-gas effect on pressure distribution was shown earlier (in connection with the Mark III vehicle, fig. 3) to be larger just behind abrupt body-surface deflections than farther downstream. The resulting effect upon forces and moments at angles of attack cannot be computed accurately for such a body of revolution, but in order to investigate this phenomenon, a computation was performed for a similar two-dimensional body for which the results would be expected to show real-gas effects qualitatively like, but much larger than, those experienced by an axisymmetric body. The configuration, shown in figure 6(a), has a wedge nose with a 30° half-angle, a slab 10 thicknesses in length, and a terminal 20° flare 5/4 of the thickness in length. The pressure distributions for M_∞ = 20 and a 200,000-foot altitude were computed by the method of characteristics for angles of attack up to the detachment angles of the nose shock for helium, perfect air, and real air. The real-air distribution was approximated by that for a perfect gas with an effective specific-heat ratio γ_e defined so that the Rankine-Hugoniot equations across the strongest shock wave in the flow field yielded the correct (real air) pressure and density. This procedure also requires use of an effective Mach number equal to $\sqrt{\dfrac{\gamma_\infty}{\gamma_e}}\,M_\infty$.

Also shown in figure 6(a) are the pressure distributions p/p_∞ plotted against ξ/t for zero angle of attack. Flare pressures were assumed to be constant at their initial values. Note the large differences in pressures just rearward of the shoulder and persisting until the first waves are reflected from the shock back to the body. Farther downstream, pressure differences between the various gases decrease, as shown in figure 3 for the Mark III body of revolution.

An example of the results obtained is shown in figure 6(b), a plot of pitching-moment coefficient (based upon overall length) against angle of attack. For the range of angle of attack shown, the configuration exhibits a positive pitching moment in all three gases; the largest values at given α are for helium up to 5°, and the smallest values are for real air. Significant real-gas effects on C_m are apparent for $5^\circ \leq \alpha \leq 15^\circ$. However, at very large angles of attack the real-gas effect should be rather small, since Newtonian pressures should be applicable. These differ for the gases only by the stagnation-pressure ratio, about a 5-percent difference between real and perfect air in this case. Flight data on the Mark III with a single-element flare showed a pitching-moment coefficient at small angles of attack qualitatively like that in figure 6(b) for real air.

Shown also in figure 6(b) is a table of static margin $\left(dC_m/dC_L \right)_{\alpha=0}$, as a fraction of body length, for the three cases. The shift in static margin from real air to perfect air is one-half of 1 percent of the body length.

It is important to note that the moment is highly dependent upon the flare location and geometry. (See fig. 6(a).) For example, if the flare of the configuration investigated were placed where the real-gas pressure was a maximum, $\xi/t \approx 7$, the flare effectiveness near $\alpha = 0$ would be little changed from the original location for the real air but much enhanced for the perfect-air and helium cases, changing the curve of C_m against α significantly.

To summarize for the inviscid flow of equilibrium air, the difference between real- and perfect-air pressure distributions and drag is at most a few percent in blunt-body nose regions, though downstream pressures on relatively slender blunted bodies may differ considerably. Because lift and moments depend on pressure differences, caution must be exercised in the interpretation of perfect-gas tests as applying to the real-gas conditions, especially for bodies having abrupt changes in surface slope and at small angles of attack. For blunt bodies of continuous slope real-gas effects are greatly reduced. Also, since sweep reduces the maximum flow-field temperatures and consequently the degree of gaseous imperfection, real-gas effects would be expected to be small for highly swept wings except at angles of attack near detachment of the wing shock.

AERODYNAMIC HEAT TRANSFER FOR EQUILIBRIUM AIR

Whereas the inviscid flow of equilibrium real air is a function of the well-tabulated thermodynamic properties and may be calculated with

some certainty, the viscous flow depends also upon the transport properties (viscosity, thermal conductivity, etc.) for which only approximations are available (e.g., refs. 17 to 19). These estimates differ, for example, by as much as 50 percent in viscosity for fully dissociated air. An important question to be considered, then, is how much are heat-transfer predictions affected by these different estimates? These predictions are limited to simple shapes where the differential equations are applicable. Because of the highly empirical nature of transition- and turbulent-flow analyses even for the perfect gas, the present discussion is limited to laminar flow.

Stagnation Flows

The stagnation boundary layers for a body of revolution and for a yawed infinite cylinder are members of the class for which exact solutions of the boundary-layer equations are possible. Correlations for the heat-transfer parameter have generally been found to be of the form

$$\left(\frac{N_{Nu,w}}{\left(N_{Pr,w}\right)^{0.4}\sqrt{N_{Re,w}}}\right)_s = A\left(\frac{\rho_e\mu_e}{\rho_w\mu_w}\right)_s^m \tag{1}$$

independent of the stagnation temperature or enthalpy level. The constants A and m depend upon the fluid properties used in solving the boundary-layer equations and the type of flow, and are listed in tables I and II for the axisymmetric stagnation point and yawed infinite cylinder, respectively. It is noteworthy that the small amount of variation in A and m shown in the tables represents solutions with fluid properties ranging from constant (incompressible fluid) to those for dissociated air computed by the present authors with the transport properties of Hansen (ref. 17). Thus the boundary-layer dimensionless parameters are hardly affected by real-gas properties.

From the definitions of the Nusselt and Reynolds numbers, the aerodynamic heat-transfer rate, using equation (1), is

$$-q_{w,s} = A\left(N_{Pr,w}\right)_s^{-.6}\left(h_{aw} - h_w\right)_s\left(\rho_e\mu_e\right)_s^m\left(\rho_w\mu_w\right)_s^{\frac{1}{2}-m}\sqrt{\left(\frac{du_e}{dx}\right)_s} \tag{2}$$

where for the axisymmetric case,

$$h_{aw} = H_e \tag{3a}$$

and for the yawed infinite cylinder,

$$h_{aw} = H_e - (1 - r) \frac{v_e^2}{2} \tag{3b}$$

and where r is the enthalpy recovery factor. Although the constants A and m are little influenced by gas properties, as shown in tables I and II, the absolute heat-transfer rate, on the other hand, may be very much influenced by the gas properties, as can be seen from equation (2). The most important factors influencing the heat-transfer rate are the stagnation-point or stagnation-line density and viscosity outside the boundary layer, $\rho_{e,s}$ and $\mu_{e,s}$, respectively. For a known real-air inviscid flow $\left(\text{known } \rho_{e,s}\right)$ the uncertainty in viscosity $\mu_{e,s}$ creates the major uncertainty in heat-transfer rate. As pointed out earlier, the viscosity for fully dissociated air may be uncertain by as much as 50 percent, but because the exponent m is near 1/2, the uncertainty in heat-transfer rate is at most about 25 percent for fully dissociated air, and even considerably less for only partial dissociation.

Up to this point, the discussion has used the assumption of unit Lewis number. For dissociating air with a constant Lewis number not equal to unity, Fay and Riddell (ref. 20) predict an effect of Lewis number given by

$$\frac{\left(N_{Nu,w}\Big/\sqrt{N_{Re,w}}\right)_{s,N_{Le}}}{\left(N_{Nu,w}\Big/\sqrt{N_{Re,w}}\right)_{s,N_{Le}=1}} = 1 + \left(N_{Le}^{0.52} - 1\right)\left(\frac{h_D}{h_e}\right)_s \tag{4}$$

which, for $N_{Le} = 1.4$, ranges from 1 for no dissociation to about 1.15 for fully dissociated air. The more recent solutions of the present authors using Hansen's transport properties (ref. 17), including variable Lewis number, give a correction factor of

$$0.98 \leq \frac{\left(N_{Nu,w}\Big/\sqrt{N_{Re,w}}\right)_{s,N_{Le}}}{\left(N_{Nu,w}\Big/\sqrt{N_{Re,w}}\right)_{s,N_{Le}=1}} \leq 1.05 \tag{5}$$

which is considered here a negligible correction.

Experimental data exist on a variety of axisymmetric nose shapes at hypersonic speeds during reentry flight tests. Shown in figure 7 are results for two shapes; the hemisphere (X-17 flights) with data obtained from references 15, 16, 21, 22, 23, and 24, and the G. E. Mark II nose cone (Atlas flights). Plotted is the ratio of experimental to theoretical real-air heat-transfer rates against flight velocity. The reference theory is that of the present authors for real air (A = 0.767, m = 0.45), but uses the more recent viscosity prediction of Bauer and Zlotnick (ref. 18) for the absolute viscosity in equation (2).

The X-17 hemisphere data scatter about the theoretical value (1.0) from 0.7 to 1.4 and the three Mark II points (three different flights, each data point at the peak heating value) scatter from 0.8 to 1.2. Shown also is a curve representing the predicted values obtained by using Fay and Riddell's correlations (A = 0.76, m = 0.4) with the Sutherland viscosity and unit Lewis number. This prediction appears low by 10 to 20 percent, but this is mainly caused by use of the Sutherland viscosity law in computing $\mu_{e,s}$ from equation (2). A correction for Lewis number effects (eq. (5)) with $N_{Le} = 1.4$, used in conjunction with the Sutherland viscosity, would bring Fay and Riddell's prediction into essential agreement with the authors'. Use of Hansen's or Bauer and Zlotnick's viscosity law for $\mu_{e,s}$ in conjunction with $N_{Le} = 1$ and Fay and Riddell's solution would also yield very good agreement, as evidenced by the small differences in A and m.

<center>Flat-Plate Flow</center>

Another exact similar solution for the laminar flow of equilibrium air exists for flat-plate boundary layers. Shown in figure 8(a) are correlations of a few of the solutions obtained by the authors with Hansen's transport property approximations for real air. Plotted here are curves of the heat-transfer parameter $N_{St}\sqrt{N_{Re}}$ against the ratio of local external $\rho\mu$ to the local wall $\rho\mu$. The parameter is the ratio of the static enthalpy to total enthalpy outside the boundary layer; the corresponding perfect-gas ($\gamma = 1.4$) external Mach numbers are also shown. As for the stagnation flow, these correlations are independent of the enthalpy level of the external flow. Plotted in the figure are some corresponding perfect-gas values (taken from Van Driest, ref. 25, and adjusted to $N_{Pr} = 0.7$), and it is seen that the real-gas effect on this parameter is at most 5 to 10 percent. As in the stagnation case, however, the absolute heat-transfer rates can be influenced by the real-gas transport properties even though the dimensionless parameters are little affected.

In the absence of flat-plate data obtained during hypersonic atmospheric flight, shock-tube data obtained on a 10° wedge by Jones (ref. 26)

are shown in figure 8(b) compared with real-air theory. Plotted is the ratio of experimental to theoretical real-air heat-transfer rate against equivalent flight velocity for the same stagnation enthalpy as in the shock-tube test. The data tend to scatter about the theory within ±20 percent. For comparison, incompressible theory (based upon real-air inviscid shock-tube conditions) is also shown and is about 10 percent lower than real-gas theory.

Laminar Heat-Transfer Distribution

The laminar heat-transfer distribution $\left(\text{the ratio } q_w/q_{w,s}\right)$ has been shown by Lees (ref. 27) to be a function only of the inviscid flow for moderately curved bodies with highly cooled walls. Typical results with Lees' method are displayed in figures 9(a) and 9(b). In figure 9(a) are shown data and theories for a hemisphere at a Mach number of 12 plotted as the ratio $q_w/q_{w,s}$ against x/R. The predicted real-gas effect is small, as expected, because the pressure distributions are so little different. The data, obtained from X-17 flight tests, scatter about both theories.

In figure 9(b) is plotted a similar figure for the G. E. Mark II nose cone. The perfect-air and real-air theoretical curves, plotted as $q_w/q_{w,s}$ against x/R_b, were computed by using Lees' method and theoretical pressure distributions shown in figure 2. Again, a small real-gas effect may be noted. The experimental data were obtained from Atlas firings and tend to scatter about the theories.

Thus, the laminar stagnation and flat-plate heat-transfer parameters, and the laminar heat-transfer distribution (ratio), are essentially unaffected by real-air properties. The heat-transfer rates themselves show a real-gas effect primarily through their dependence upon the local inviscid flow and transport properties, but are generally predictable within the scatter of experimental data.

NONEQUILIBRIUM EFFECTS

The theory of finite-rate processes is in its infancy at the present time and various estimates of the reaction-rate parameters differ by orders of magnitude. Some estimates of characteristic relaxation lengths have been made; for example, the dissociation and vibration relaxation lengths are sufficiently short for chemical equilibrium to be assumed for flow behind normal shocks with $M_\infty > 15$ below 250,000 feet of altitude if the characteristic flow length is 1 foot (ref. 28). On

the other hand, for an oblique shock with a flow deflection angle of 25° at $M_\infty = 22$, nonequilibrium effects may enter above about 150,000 feet of altitude (ref. 28). In any event, finite-rate pressures immediately behind <u>all</u> portions of the primary shock wave should be roughly between the extremes predicted by perfect (frozen) and equilibrium real-air computations (seen previously to be at most of the order of 20 percent). Surface pressures close to the stagnation point will also be within the perfect and equilibrium real-air pressures, that is, within relatively narrow limits (around 5 percent).

Less can be said regarding downstream effects of finite relaxation rates. It is clear that in regions of rapid expansion, such as near the vertex of a Prandtl-Meyer expansion fan, nonequilibrium rates may cause relatively large local pressure disturbances, but the effects upon body forces and moments cannot be estimated. Separation and reattachment might be strongly affected by finite rates, as illustrated qualitatively in figure 10. Shown is the corner region of a typical ballistic capsule. Separation was assumed to occur at the rearward corner, and the flow was then assumed to expand to a given pressure (corresponding to flight measurements) for perfect air, and for frozen and equilibrium real air. The initial slope of the separation streamline shown in the figure, and hence flow reattachment on the afterbody, is seen to depend strongly upon the assumed reaction rates. Corners and afterbodies of this type occur on the G. E. Mark II and Mercury capsules. It is interesting that no reattachment was observed during Mark II flights, although an equilibrium expansion around the corners to the measured afterbody pressure indicated the likelihood of flow reattachment.

Nonequilibrium effects upon heat-transfer dimensionless parameters have been shown by Fay and Riddell (ref. 20) and by Chung and Anderson (ref. 29), to be negligible for stagnation and flat-plate flows, respectively, provided the wall is cold and catalytic. If the wall were non-catalytic, on the other hand, significant reductions in heat transfer could be obtained with cold walls, because some of the energy of dissociation would be retained by those atoms not recombining at the surface.

CONCLUSIONS

It has been shown that equilibrium real-gas behavior does not, in general, drastically affect inviscid flow forces and moments and aerodynamic heat-transfer rates for most of the simple shapes considered. In fact, the scatter in the real-air experimental pressure and heat-transfer data on these shapes was shown to be larger than the predicted real-gas effect. Significant real-gas effects in inviscid flow were predicted only for some unswept two-dimensional shapes having discontinuities in surface slope at small angles of attack, and for swept flat plates near the shock detachment angle.

On the basis of the results obtained on most of the simple shapes considered here, real-gas effects are expected to be small on the more complicated configurations presently being investigated for use as reentry vehicles, because these shapes are characterized by highly swept surfaces and are designed, for the most part, for flight at relatively high angles of attack. It therefore appears that for such configurations where performance cannot be computed accurately for either real or perfect air, perfect-gas tests, used in conjunction with those analytic studies which are possible, will provide useful design data for flight conditions where equilibrium real-gas behavior is expected.

Lastly, nonequilibrium effects on inviscid flow appear important mainly in regions immediately downstream of rapid expansions. With cold, catalytic walls, the heat-transfer parameters are essentially independent of finite rate processes.

L
1
0
5
0

REFERENCES

1. Gilmore, F. R.: Equilibrium Composition and Thermodynamic Properties of Air to 24,000° K. U.S. Air Force Project RAND Res. Memo. RM-1543, The RAND Corp., Aug. 24, 1955. (Also Available From ASTIA as AD-84052.)

2. Hilsenrath, Joseph, and Beckett, Charles W.: Tables of Thermodynamic Properties of Argon-Free Air to 15,000° K. AEDC-TN-56-12, Arnold Eng. Dev. Center, Sept. 1956. (Also Available From ASTIA as Doc. No. AD-98974.)

3. Treanor, C. E., and Logan, J. G., Jr.: Tables of Thermodynamic Properties of Air From 3,000° K to 10,000° K. Rep. No. AD-1052-A-2 (Contract No. AF 40(600)-6, AF 18(603)-10), Cornell Aero. Lab., Inc., June 1956.

4. Feldman, Saul: Hypersonic Gas Dynamic Charts for Equilibrium Air. AVCO Res. Lab., Jan. 1957.

5. Moeckel, W. E., and Weston, Kenneth C.: Composition and Thermodynamic Properties of Air in Chemical Equilibrium. NACA TN 4265, 1958.

6. Gravalos, F. G., Edelfelt, I. H., and Emmons, H. W.: The Supersonic Flow About a Blunt Body of Revolution for Gases at Chemical Equilibrium. Doc. No. R58SD245, Missile and Ord. Syst. Dept., Gen. Elec. Co., June 16, 1958.

7. Holt, Maurice: Calculation of Pressure Distribution on Hypersonic Bodies of Revolution by Belotserkovskii's Method. RAD-2-TM-58-45, AVCO Res. and Advanced Dev. Div., Mar. 31, 1958 (Reissued Sept. 30, 1959).

8. Van Dyke, Milton D.: The Supersonic Blunt-Body Problem - Review and Extension. Jour. Aero/Space Sci., vol. 25, no. 8, Aug. 1958, pp. 485-496.

9. Vaglio-Laurin, Roberto, and Ferri, Antonio: Theoretical Investigation of the Flow Field About Blunt-Nosed Bodies in Supersonic Flight. Jour. Aero/Space Sci., vol. 25, no. 12, Dec. 1958, pp. 761-770.

10. Beckwith, Ivan E., and Gallagher, James J.: Heat Transfer and Recovery Temperatures on a Sphere With Laminar, Transitional, and Turbulent Boundary Layers at Mach Numbers of 2.00 and 4.15. NACA TN 4125, 1957.

L
1
0
5
0

11. Lehnert, R., and Schermerhorn, V. L.: Wake Investigation on Sharp and Blunt Nose Cones at Supersonic Speeds. NAVORD Rep. 5668, U.S. Naval Ord. Lab. (White Oak, Md.), Jan. 28, 1958.

12. Cooper, Morton, and Mayo, Edward E.: Measurements of Local Heat Transfer and Pressure on Six 2-Inch-Diameter Blunt Bodies at a Mach Number of 4.95 and at Reynolds Numbers Per Foot up to 81×10^6. NASA MEMO 1-3-59L, 1959.

13. Oliver, Robert E.: An Experimental Investigation of Flow Over Simple Blunt Bodies at a Nominal Mach Number of 5.8. GALCIT Memo. No. 26 (Contract No. DA-04-495-Ord-19), June 1, 1955.

14. Crawford, Davis H., and McCauley, William D.: Investigation of the Laminar Aerodynamic Heat-Transfer Characteristics of a Hemisphere-Cylinder in the Langley 11-Inch Hypersonic Tunnel at a Mach Number of 6.8. NACA Rep. 1323, 1957. (Supersedes NACA TN 3706.)

15. X-17 Re-Entry Test Vehicle - R-22 Final Flight Report. Rep. LMSD-3042, Lockheed Aircraft Corp., May 14, 1957.

16. X-17 Re-Entry Test Vehicle - R-26 Final Flight Report. Rep. LMSD-2600, Lockheed Aircraft Corp., Nov. 22, 1957.

17. Hansen, C. Frederick: Approximations for the Thermodynamic and Transport Properties of High-Temperature Air. NACA TN 4150, 1958.

18. Bauer, Ernest, and Zlotnick, Martin: Transport Coefficients of Air to 8,000° K. RAD-TR-58-12, AVCO Res. and Advanced Dev. Div., Sept. 29, 1958.

19. Green, Melville S.: The Transport Properties of Air at Elevated Temperatures. Viscosity, Thermal Conductivity, and Prandtl Number of Air From 1,000° K to 10,000° K at Normal Densities of 1, .1, and .01. Unpublished Report, Nat. Bur. Standards, 1957.

20. Fay, J. A., and Riddell, F. R.: Theory of Stagnation Point Heat Transfer in Dissociated Air. Jour. Aero. Sci., vol. 25, no. 2, Feb. 1958, pp. 73-85, 121.

21. X-17 Re-Entry Test Vehicle - R-2 Final Flight Report. Rep. MSD-3003, Lockheed Aircraft Corp., Oct. 17, 1956.

22. X-17 Re-Entry Test Vehicle - R-8 Final Flight Report. Rep. MSD-3028, Lockheed Aircraft Corp., Jan. 1, 1957.

23. X-17 Re-Entry Test Vehicle - R-9 Final Flight Report. Rep. MSD-3029, Lockheed Aircraft Corp., Jan. 5, 1957.

L
1
0
5
0

24. X-17 Re-Entry Test Vehicle - R-11 Final Flight Report. Rep. MSD-3031, Lockheed Aircraft Corp., Jan. 18, 1957.

25. Van Driest, E. R.: Investigation of Laminar Boundary Layer in Compressible Fluids Using the Crocco Method. NACA TN 2597, 1952.

26. Jones, Jim J.: Resumé of Experiments Conducted in the High-Pressure Shock Tube of the Gas Dynamics Laboratory at NASA. Proc. Third Shock Tube Symposium. SWR-TM-59-2, Air Force Special Weapons Center, Mar. 10-12, 1959.

27. Lees, Lester: Laminar Heat Transfer Over Blunt-Nosed Bodies at Hypersonic Flight Speeds. Jet Propulsion, vol. 26, no. 4, Apr. 1956, pp. 259-269.

28. Anon.: Aerodynamics Report. Vol. II. ER 10372 (Contract No. AF 33(600)-37705), Martin Space Flight, Mar. 1959.

29. Chung, Paul M., and Anderson, Aemer D.: Dissociative Relaxation of Oxygen Over an Adiabatic Flat Plate at Hypersonic Mach Numbers. NASA TN D-140, 1960.

30. Sibulkin, M.: Heat Transfer Near the Forward Stagnation Point of a Body of Revolution. Jour. Aero. Sci. (Readers' Forum), vol. 19, no. 8, Aug. 1952, pp. 570-571.

31. Beckwith, Ivan E.: Similar Solutions for the Compressible Boundary Layer on a Yawed Cylinder With Transpiration Cooling. NASA TR R-42, 1959. (Supersedes NACA TN 4345.)

32. Kemp, Nelson H., Rose, Peter H., and Detra, Ralph W.: Laminar Heat Transfer Around Blunt Bodies in Dissociated Air. Jour. Aero/Space Sci., vol. 26, no. 7, July 1959, pp. 421-430.

33. Fluid Motion Panel of the Aeronautical Research Committee and Others: Modern Developments in Fluid Dynamics. Vol. II, ch. XIV, sec. 270, S. Goldstein, ed., The Clarendon Press (Oxford), 1938, p. 631.

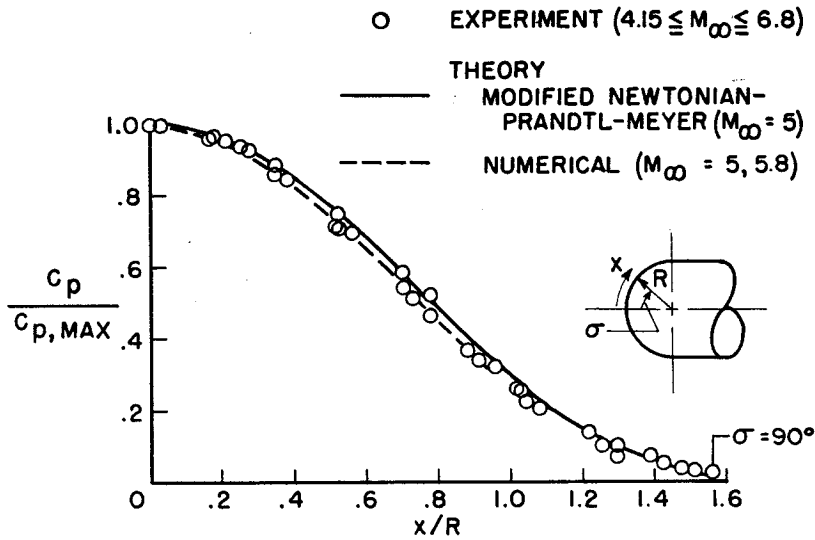## HEMISPHERE PRESSURE-COEFFICIENT DISTRIBUTIONS
LOW MACH NUMBER

O   EXPERIMENT $(4.15 \leqq M_\infty \leqq 6.8)$

THEORY

——— MODIFIED NEWTONIAN-
PRANDTL-MEYER $(M_\infty = 5)$

– – – NUMERICAL $(M_\infty = 5, 5.8)$

Figure 1(a)

HEMISPHERE PRESSURE-COEFFICIENT DISTRIBUTIONS
HIGH MACH NUMBER

O   X-17 DATA $(M_\infty = 12)$

THEORY

——— MODIFIED NEWTONIAN-PRANDTL-MEYER $(M_\infty = 12, \gamma = 1.195)$

– – – GRAVALOS REAL AIR, FROM G.E. $(M_\infty = 15, C_D = 0.904)$

—·—· GRAVALOS PERFECT GAS, FROM G.E. $(M_\infty = 15, C_D = 0.882)$

M_∞	$C_{p, MAX}$ (PERFECT)	$C_{p, MAX}$ (REAL)
12	1.83	1.89
15	1.84	1.91
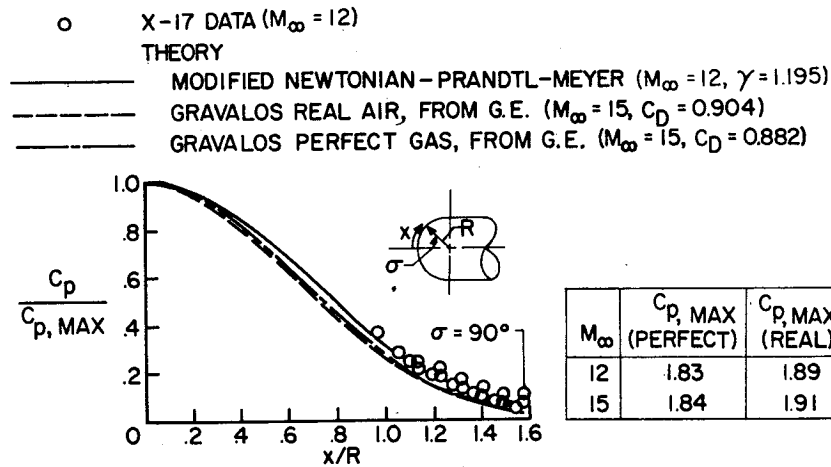
Figure 1(b)

PRESSURE-COEFFICIENT DISTRIBUTIONS ON ATLAS MARK II

		ALTITUDE, FT	M_∞
o	FLIGHT DATA	74,000 TO 102,000	11.1 TO 16.7
	GRAVALOS THEORY (FROM G.E.)		
——	REAL AIR	270,000	14.6
-----	REAL AIR	90,000	10.5
—·—	PERFECT GAS	ALL	15.0
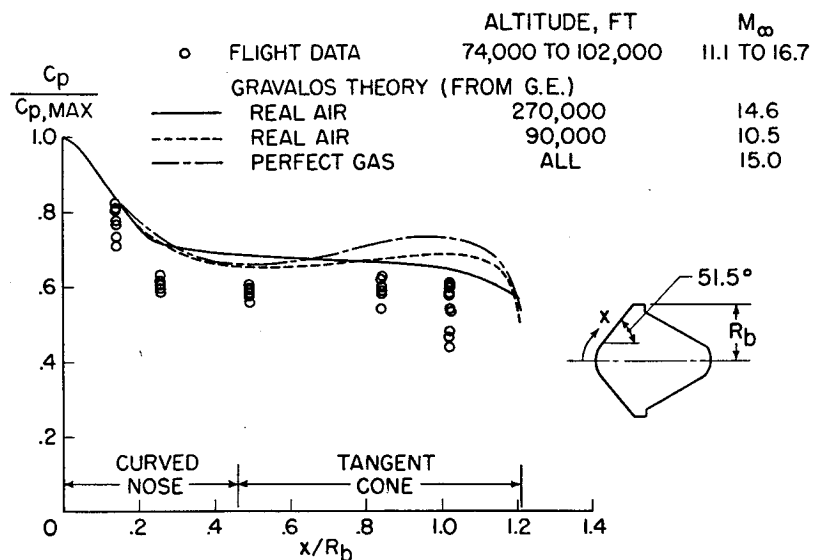
Figure 2

PRESSURE - COEFFICIENT DISTRIBUTION ON ATLAS MARK III
$M_\infty = 20$

GRAVALOS THEORY (FROM GENERAL ELECTRIC)		ALTITUDE, FT	$c_{p, MAX}$
——	REAL AIR	200,000	1.93
----	REAL AIR	60,430	1.91
—·—	PERFECT GAS	ALL	1.84
I	FLIGHT DATA	62,000	
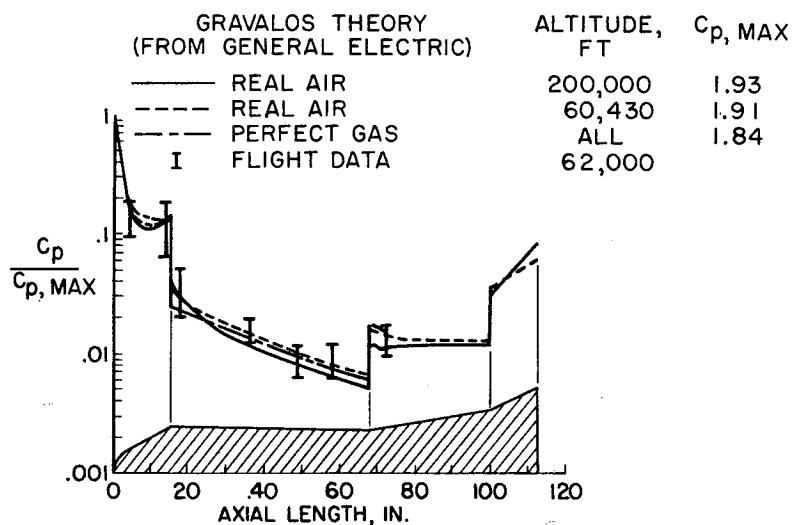
Figure 3

RATIO OF PERFECT TO REAL-AIR SURFACE PRESSURE
SWEPT FLAT PLATES AT ANGLE OF ATTACK; $M_\infty = 20$; ALTITUDE, 200,000 FT
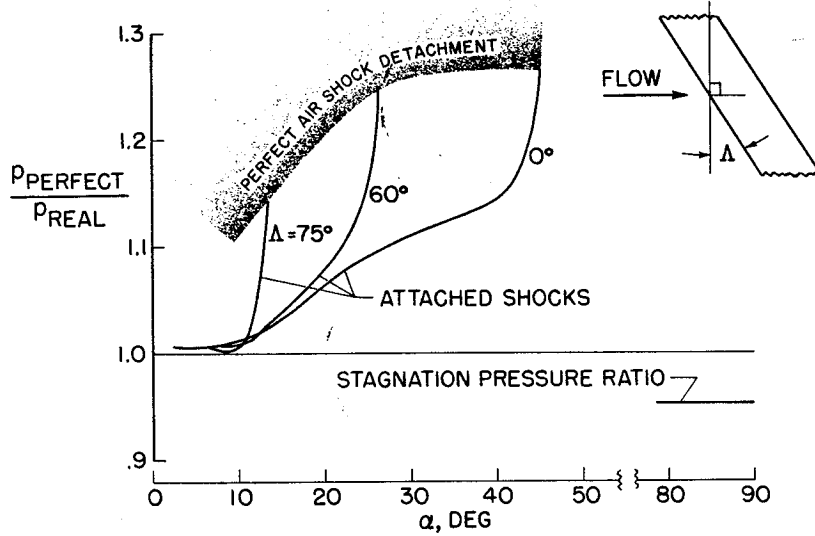
Figure 4

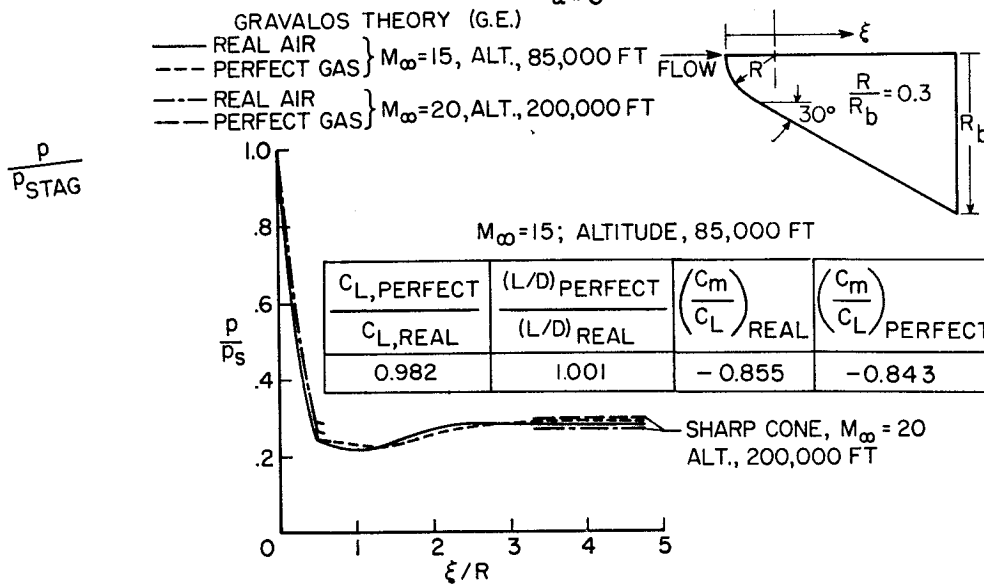## AERODYNAMIC CHARACTERISTICS OF A BLUNTED HALF-CONE
$\alpha = 0°$

GRAVALOS THEORY (G.E.)

—— REAL AIR } $M_\infty = 15$, ALT., 85,000 FT
——— PERFECT GAS

—·— REAL AIR } $M_\infty = 20$, ALT., 200,000 FT
—— PERFECT GAS

$M_\infty = 15$; ALTITUDE, 85,000 FT

$\dfrac{C_{L,PERFECT}}{C_{L,REAL}}$	$\dfrac{(L/D)_{PERFECT}}{(L/D)_{REAL}}$	$\left(\dfrac{C_m}{C_L}\right)_{REAL}$	$\left(\dfrac{C_m}{C_L}\right)_{PERFECT}$
0.982	1.001	−0.855	−0.843

Figure 5

PRESSURE DISTRIBUTIONS FOR ILLUSTRATIVE
TWO DIMENSIONAL CONFIGURATION
$M_\infty = 20$; ALTITUDE, 200,000 FT; $\alpha = 0$
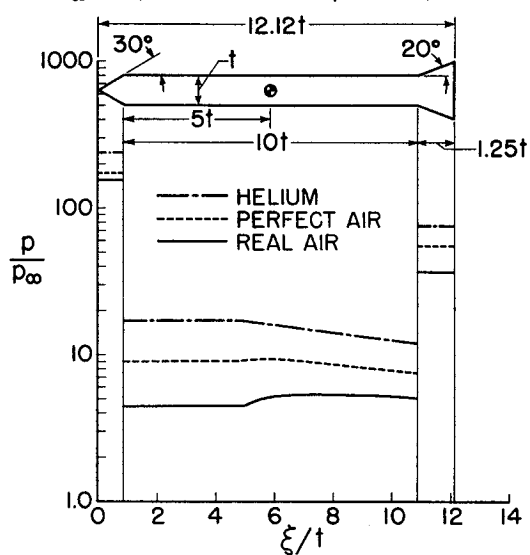
Figure 6(a)

PITCHING MOMENT COEFFICIENT FOR ILLUSTRATIVE
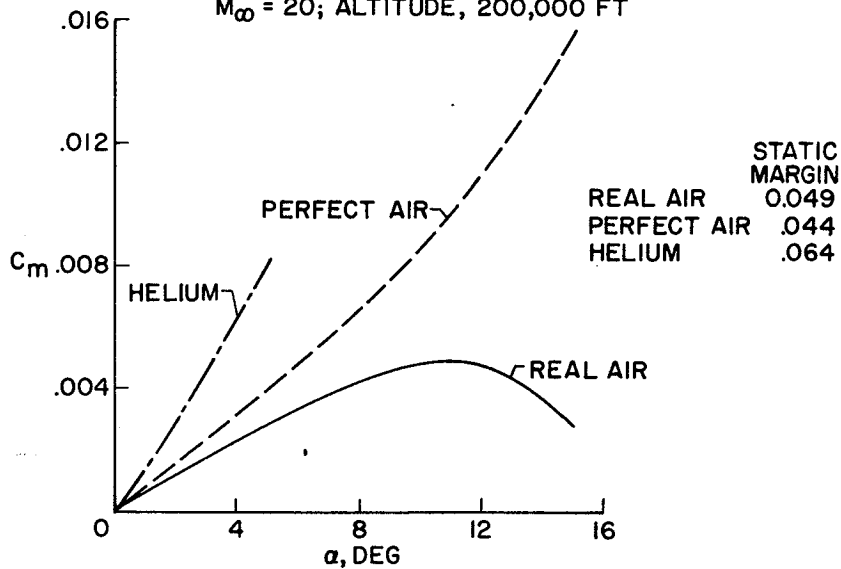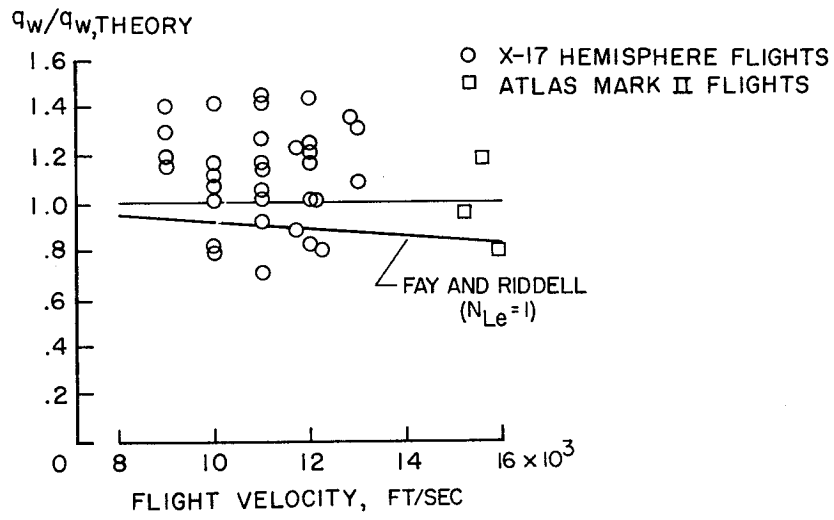TWO-DIMENSIONAL CONFIGURATION
$M_\infty = 20$; ALTITUDE, 200,000 FT

	STATIC MARGIN
REAL AIR	0.049
PERFECT AIR	.044
HELIUM	.064

Figure 6(b)

STAGNATION-POINT HEAT-TRANSFER RATES FOR A
BODY OF REVOLUTION

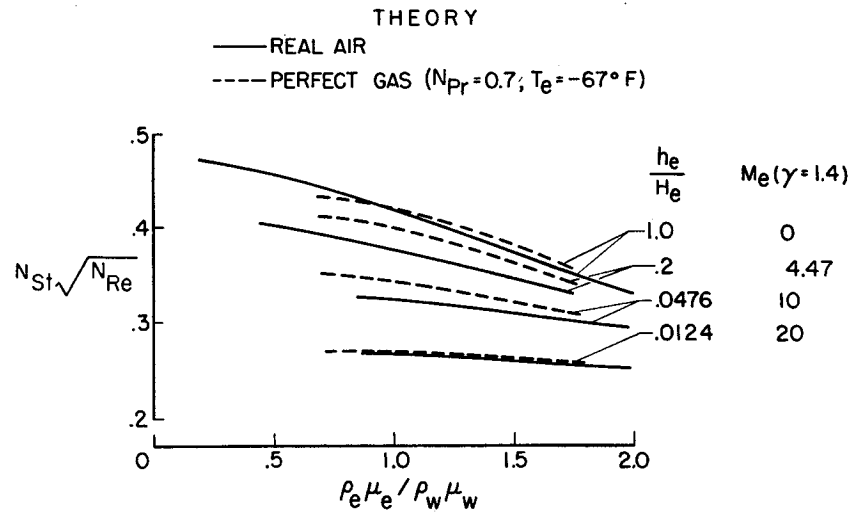Figure 7

REAL-AIR LAMINAR-HEAT-TRANSFER PARAMETER FOR A FLAT PLATE

THEORY
——REAL AIR
----PERFECT GAS (N_{Pr}=0.7, T_e=-67°F)

$N_{St}\sqrt{N_{Re}}$

$\dfrac{h_e}{H_e}$ $M_e(\gamma=1.4)$

1.0   0
.2   4.47
.0476   10
.0124   20

$\rho_e\mu_e/\rho_w\mu_w$

Figure 8(a)

HEAT TRANSFER FOR A 10° WEDGE IN SHOCK-TUBE FLOW

$\dfrac{q_w}{q_{w,\,THEORY}}$

INCOMPRESSIBLE, N_{Pr}=0.7

EQUIVALENT FLIGHT VELOCITY, FT/SEC

Figure 8(b)

358
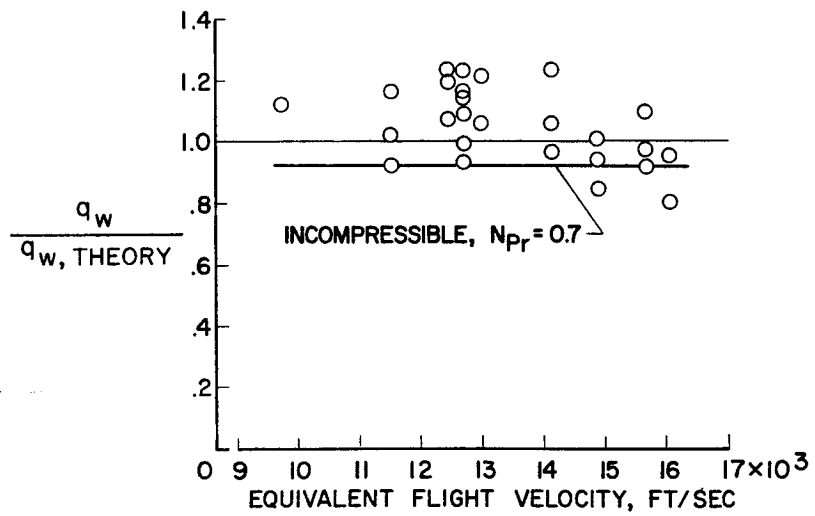
HEAT-TRANSFER DISTRIBUTIONS ON A HEMISPHERE
$M_\infty \approx 12$
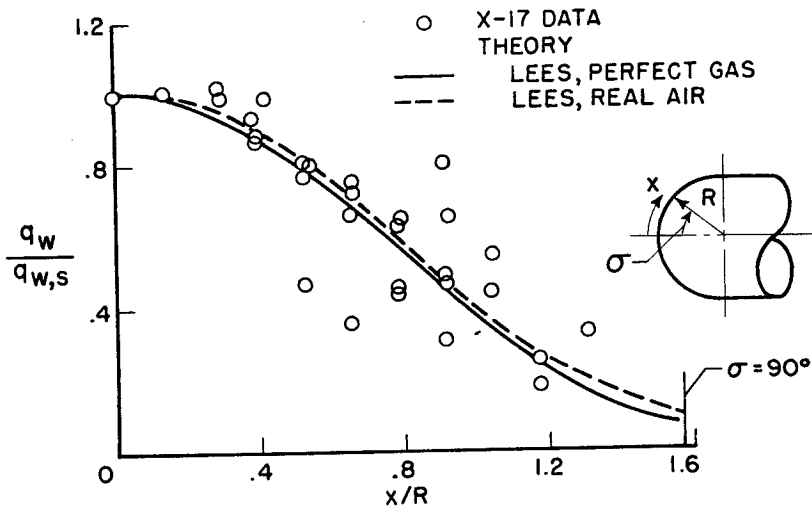
Figure 9(a)
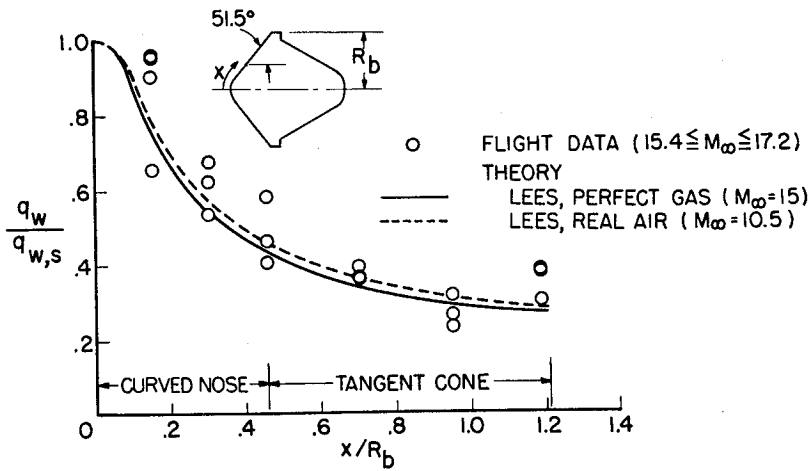
HEAT-TRANSFER DISTRIBUTION ON ATLAS MARK II

Figure 9(b)

NONEQUILIBRIUM EFFECT ON AFTERBODY FLOW

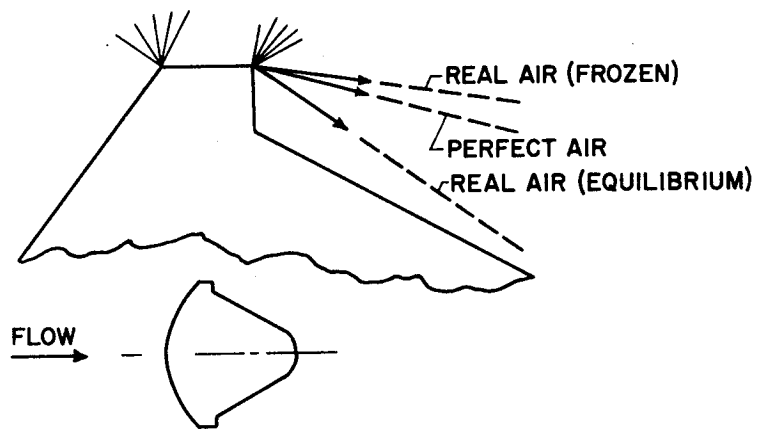$M_\infty = 20$; ALTITUDE, 200,000 FT

Figure 10